The Astrophysical Journal, 903:75 (10pp), 2020 November 1 https://doi.org/10.3847/1538-4357/abb823


# A DESGW Search for the Electromagnetic Counterpart to the LIGO/Virgo Gravitational-wave Binary Neutron Star Merger Candidate S190510g

A. Garcia[1], R. Morgan[2], K. Herner[3], A. Palmese[3,4], M. Soares-Santos[1], J. Annis[3], D. Brout[5], A. K. Vivas[6], A. Drlica-Wagner[3,4,7], L. Santana-Silva[8], D. L. Tucker[3], S. Allam[3], M. Wiesner[9], J. García-Bellido[10], M. S. S. Gill[11], M. Sako[5], R. Kessler[4,7], T. M. Davis[12], D. Scolnic[13], J. Casares[14], H. Chen[4], C. Conselice[15], J. Cooke[16], Z. Doctor[4], R. J. Foley[17], J. Horvath[18], D. A. Howell[19], C. D. Kilpatrick[20], C. Lidman[21], F. Olivares E.[22], F. Paz-Chinchón[23,24], J. Pineda-G.[25], J. Quirola-Vásquez[26,27], A. Rest[28], N. Sherman[1], T. M. C. Abbott[6], M. Aguena[29,30], S. Avila[10], E. Bertin[31,32], S. Bhargava[33], D. Brooks[34], D. L. Burke[11,35], A. Carnero Rosell[36,37], M. Carrasco Kind[24,38], J. Carretero[39], M. Costanzi[40,41], L. N. da Costa[30,42], S. Desai[43], H. T. Diehl[3], J. P. Dietrich[44], P. Doel[34], S. Everett[17], B. Flaugher[3], P. Fosalba[45,46], D. Friedel[24], J. Frieman[3,4], E. Gaztanaga[45,46], D. W. Gerdes[47,48], D. Gruen[11,35,49], R. A. Gruendl[24,38], J. Gschwend[30,42], G. Gutierrez[3], S. R. Hinton[12], D. L. Hollowood[17], K. Honscheid[50,51], D. J. James[52], K. Kuehn[53,54], N. Kuropatkin[3], O. Lahav[34], M. Lima[29,30], M. A. G. Maia[30,42], M. March[5], J. L. Marshall[55], F. Menanteau[24,38], R. Miquel[39,56], R. L. C. Ogando[30,42], A. A. Plazas[57], A. K. Romer[33], A. Roodman[11,35], E. Sanchez[58], V. Scarpine[3], M. Schubnell[48], S. Serrano[45,46], I. Sevilla-Noarbe[58], M. Smith[59], E. Suchyta[60], M. E. C. Swanson[24], G. Tarle[48], D. Thomas[61], T. N. Varga[62,63], A. R. Walker[6], and J. Weller[62,63]

(DES Collaboration)

[1] Brandeis University, Physics Department, 415 South Street, Waltham, MA 02453, USA; alyssag94@brandeis.edu
[2] Physics Department, 2320 Chamberlin Hall, University of Wisconsin–Madison, 1150 University Avenue, Madison, WI 53706-1390, USA
[3] Fermi National Accelerator Laboratory, P.O. Box 500, Batavia, IL 60510, USA
[4] Kavli Institute for Cosmological Physics, University of Chicago, Chicago, IL 60637, USA
[5] Department of Physics and Astronomy, University of Pennsylvania, Philadelphia, PA 19104, USA
[6] Cerro Tololo Inter-American Observatory, NSF's National Optical-Infrared Astronomy Research Laboratory, Casilla 603, La Serena, Chile
[7] Department of Astronomy and Astrophysics, University of Chicago, Chicago, IL 60637, USA
[8] Federal University of Rio de Janeiro, Valongo Observatory, Rio de Janeiro, Brazil
[9] Benedictine University, Lisle, IL 60532, USA
[10] Instituto de Fisica Teorica UAM/CSIC, Universidad Autonoma de Madrid, E-28049 Madrid, Spain
[11] SLAC National Accelerator Laboratory, Menlo Park, CA 94025, USA
[12] School of Mathematics and Physics, University of Queensland, Brisbane, QLD 4072, Australia
[13] Department of Physics, Duke University, Durham, NC 27708, USA
[14] Instituto de Astrofisica de Caanarias (IAC), Santa Cruz de Tenerife, Spain
[15] University of Nottingham, School of Physics and Astronomy, Nottingham NG7 2RD, UK
[16] Swinburne University, Melbourne, Australia
[17] Santa Cruz Institute for Particle Physics, Santa Cruz, CA 95064, USA
[18] Instituto de Astronomia, Geofísica e Ciências Atmosféricas (IAG), Universidade de São Paulo (USP), São Paulo, Brazil
[19] Las Cumbres Observatory, Santa Barbra, CA, USA
[20] University of California, Santa Cruz, Santa Cruz, CA, 95064, USA
[21] The Research School of Astronomy and Astrophysics, Australian National University, Canberra, ACT 2601, Australia
[22] Instituto de Astronomía y Ciencias Planetarias, Universidad de Atacama, Copayapu 485, Copiapó, Chile
[23] Institute of Astronomy, University of Cambridge, Madingley Road, Cambridge CB3 0HA, UK
[24] National Center for Supercomputing Applications, 1205 West Clark Street, Urbana, IL 61801, USA
[25] Departamento de Ciencias Físicas, Universidad Andrés Bello, Avda. Repblica 252, Santiago de Chile, Chile
[26] Instituto de Astrofísica, Pontificia Universidad Católica de Chile, Casilla 306, Santiago 22, Chile
[27] Institute of Astrophysics (MAS), Nuncio Monseñor Sótero Sanz 100, Providencia, Santiago, Chile
[28] Space Telescope Science Institute/Johns Hopkins University, Baltimore, MD 21218, USA
[29] Departamento de Física Matemática, Instituto de Física, Universidade de São Paulo, CP 66318, São Paulo, SP—05314-970, Brazil
[30] Laboratório Interinstitucional de e-Astronomia—LIneA, Rua Gal. José Cristino 77, Rio de Janeiro, RJ—20921-400, Brazil
[31] CNRS, UMR 7095, Institut d'Astrophysique de Paris, F-75014 Paris, France
[32] Sorbonne Universités, UPMC Univ Paris 06, UMR 7095, Institut d'Astrophysique de Paris, F-75014, Paris, France
[33] Department of Physics and Astronomy, Pevensey Building, University of Sussex, Brighton BN1 9QH, UK
[34] Department of Physics & Astronomy, University College London, Gower Street, London WC1E 6BT, UK
[35] Kavli Institute for Particle Astrophysics & Cosmology, P.O. Box 2450, Stanford University, Stanford, CA 94305, USA
[36] Instituto de Astrofísica de Canarias, E-38205 La Laguna, Tenerife, Spain
[37] Departamento de Astrofísica, Universidad de La Laguna, E-38206 La Laguna, Tenerife, Spain
[38] Department of Astronomy, University of Illinois at Urbana-Champaign, 1002 W. Green Street, Urbana, IL 61801, USA
[39] Institut de Física d'Altes Energies (IFAE), The Barcelona Institute of Science and Technology, Campus UAB, E-08193 Bellaterra (Barcelona), Spain
[40] INAF-Osservatorio Astronomico di Trieste, via G.B. Tiepolo 11, I-34143 Trieste, Italy
[41] Institute for Fundamental Physics of the Universe, Via Beirut 2, I-34014 Trieste, Italy
[42] Observatório Nacional, Rua Gal. José Cristino 77, Rio de Janeiro, RJ—20921-400, Brazil
[43] Department of Physics, IIT Hyderabad, Kandi, Telangana 502285, India
[44] Faculty of Physics, Ludwig-Maximilians-Universität, Scheinerstr. 1, D-81679 Munich, Germany
[45] Institut d'Estudis Espacials de Catalunya (IEEC), E-08034 Barcelona, Spain
[46] Institute of Space Sciences (ICE, CSIC), Campus UAB, Carrer de Can Magrans, s/n, E-08193 Barcelona, Spain
[47] Department of Astronomy, University of Michigan, Ann Arbor, MI 48109, USA
[48] Department of Physics, University of Michigan, Ann Arbor, MI 48109, USA
[49] Department of Physics, Stanford University, 382 Via Pueblo Mall, Stanford, CA 94305, USA
[50] Center for Cosmology and Astro-Particle Physics, The Ohio State University, Columbus, OH 43210, USA
[51] Department of Physics, The Ohio State University, Columbus, OH 43210, USA

[52] Center for Astrophysics | Harvard & Smithsonian, 60 Garden Street, Cambridge, MA 02138, USA
[53] Australian Astronomical Optics, Macquarie University, North Ryde, NSW 2113, Australia
[54] Lowell Observatory, 1400 Mars Hill Road, Flagstaff, AZ 86001, USA
[55] George P. and Cynthia Woods Mitchell Institute for Fundamental Physics and Astronomy, and Department of Physics and Astronomy, Texas A&M University, College Station, TX 77843, USA
[56] Institució Catalana de Recerca i Estudis Avançats, E-08010 Barcelona, Spain
[57] Department of Astrophysical Sciences, Princeton University, Peyton Hall, Princeton, NJ 08544, USA
[58] Centro de Investigaciones Energéticas, Medioambientales y Tecnológicas (CIEMAT), Madrid, Spain
[59] School of Physics and Astronomy, University of Southampton, Southampton SO17 1BJ, UK
[60] Computer Science and Mathematics Division, Oak Ridge National Laboratory, Oak Ridge, TN 37831, USA
[61] Institute of Cosmology and Gravitation, University of Portsmouth, Portsmouth PO1 3FX, UK
[62] Max Planck Institute for Extraterrestrial Physics, Giessenbachstrasse, D-85748 Garching, Germany
[63] Universitäts-Sternwarte, Fakultät für Physik, Ludwig-Maximilians Universität München, Scheinerstr. 1, D-81679 München, Germany
*Received 2020 July 8; revised 2020 September 9; accepted 2020 September 11; published 2020 November 3*

## Abstract

We present the results from a search for the electromagnetic counterpart of the LIGO/Virgo event S190510g using the Dark Energy Camera (DECam). S190510g is a binary neutron star (BNS) merger candidate of moderate significance detected at a distance of 227 ± 92 Mpc and localized within an area of 31 (1166) square degrees at 50% (90%) confidence. While this event was later classified as likely nonastrophysical in nature within 30 hours of the event, our short latency search and discovery pipeline identified 11 counterpart candidates, all of which appear consistent with supernovae following offline analysis and spectroscopy by other instruments. Later reprocessing of the images enabled the recovery of six more candidates. Additionally, we implement our candidate selection procedure on simulated kilonovae and supernovae under DECam observing conditions (e.g., seeing and exposure time) with the intent of quantifying our search efficiency and making informed decisions on observing strategy for future similar events. This is the first BNS counterpart search to employ a comprehensive simulation-based efficiency study. We find that using the current follow-up strategy, there would need to be 19 events similar to S190510g for us to have a 99% chance of detecting an optical counterpart, assuming a GW170817-like kilonova. We further conclude that optimization of observing plans, which should include preference for deeper images over multiple color information, could result in up to a factor of 1.5 reduction in the total number of follow-ups needed for discovery.

*Unified Astronomy Thesaurus concepts:* Gravitational wave astronomy (675)

## 1. Introduction

Binary neutron star mergers such as GW170817 (Abbott et al. 2017c), in which both a gravitational wave and its electromagnetic counterpart were detected, can be used for measurements such as an independent calculation of the Hubble constant (Schutz 1986; Del Pozzo 2012; Abbott et al. 2017b; Soares-Santos et al. 2019; Palmese et al. 2020a), or even to probe the growth of structure from peculiar velocities (Palmese & Kim 2020). For this reason, the Dark Energy Survey (DES; Dark Energy Survey Collaboration et al. 2016) launched the gravitational-wave (GW) program (DESGW) in 2015. This program works to quickly identify the optical counterparts to GW events, particularly the kilonovae (KN) expected from binary neutron star mergers to be used for cosmology. These transients are produced by the radioactive decay of *r*-process nuclei synthesized in the merger ejecta and are predicted to be rapidly fading (typically within a few days; Kasen et al. 2017), thus requiring follow-up shortly after the announcement of the trigger. The identification of the KN associated with GW170817 (Abbott et al. 2017a; Andreoni et al. 2017; Coulter et al. 2017; Cowperthwaite et al. 2017; Evans et al. 2017; Hu et al. 2017; Kasliwal et al. 2017; McCully et al. 2017; Shappee et al. 2017; Soares-Santos et al. 2017; Utsumi et al. 2017; Valenti et al. 2017) in the nearby galaxy NGC 4993 (Blanchard et al. 2017; Palmese et al. 2017) is an example of DESGW's ability to quickly identify these transients and characterize them.

The Laser Interferometer Gravitational-wave Observatory (LIGO; Aasi et al. 2015) and Virgo (Caron et al. 1999) Collaboration (LVC) recently completed its third observing run (O3), from 2019 April through 2020 March. During this time, there were 56 publicly reported GW candidates, 14 of which were thought to have originated from binary systems where at least one object's mass was consistent with a neutron star. In previous LVC observing runs, 11 total events (confirmed GW and marginal triggers) were observed within roughly 14 months (Abbott et al. 2019). The increase in number of GW triggers in O3 relative to earlier runs is due to a significant increase in sensitivity (Abbott et al. 2018a) for all three detectors. This also means that, while the LVC network is detecting more events, many of these events are further away than the first two runs and poorly localized.

While the optical counterparts of these events are challenging to detect with small telescopes, the Dark Energy Camera (DECam; Flaugher et al. 2015) is optimally suited to find these sources (as shown in Soares-Santos et al. 2016, 2017). DECam's 4 m primary mirror allows us to quickly cover large areas of sky down to the limits required to detect electromagnetic (EM) counterparts of LVC's sources. DECam has been widely used by the community to search for GW counterpart searches. For example, the Global Relay of Observatories Watching Transients Happen (GROWTH; Goldstein et al. 2019; Andreoni et al. 2020a) collaboration has employed DECam data wide-area searches for several GW candidate events, including S190510g (Andreoni et al. 2019b). None of the search teams have identified a new GW event counterpart since GW170817. In order to interpret the lack of detection, and make informed decisions for future searches, an in-depth analysis including a simulation-based efficiency study is required. General studies using average depth have been

published (Carracedo et al. 2020), as well as studies using similar simulation-based methods (Andreoni et al. 2020b; Kasliwal et al. 2020). See also our companion paper on GW190814, a potential neutron star black hole event (Morgan et al. 2020).

In this paper we present the DESGW search for the KN counterpart to LVC candidate event S190510g. We include results from simulations that allow us to make quantitative statements about sensitivity in light of realistic observing conditions and strategy choices. The paper is organized as follows. In Section 2 we summarize the search and discovery pipeline used by the DESGW program and give an overview of the candidates discovered. In Section 3 we discuss the method for detecting candidates and for using simulated supernova (SN) and KN light curves. In Section 4 we present the results of our search and discovery pipeline as well as a simulation analysis. Section 5 discusses our search efficiency and implications for future follow-up strategies. Finally, we summarize our analysis in Section 6.

## 2. Data

### 2.1. The LIGO/Virgo Event S190510g

All three LVC detectors (LIGO Livingston, LIGO Hanford, and Virgo) recorded the event, with a 98% initial probability of being a binary neutron star (BNS) event, a 2% probability of having a nonastrophysical origin, and a false alarm rate of 1 per 37 yr. The 50% (90%) confidence regions spanned 575 $\mathrm{deg}^2$ (3462 $\mathrm{deg}^2$) in the initial LVC bayestar localization map. At 10:08:19 UTC on May 10, the LVC released an updated map from the LaLInference pipeline (Veitch et al. 2015), decreasing the 50% and 90% confidence regions to 31 $\mathrm{deg}^2$ and 1166 $\mathrm{deg}^2$, respectively, and refined the distance estimate to $227 \pm 92$ Mpc, or $z = 0.05 \pm 0.02$ (using flat ΛCDM cosmology with $H_0 = 70$ km $\mathrm{s}^{-1}$ $\mathrm{Mpc}^{-1}$ and $\Omega_m = 0.3$) (LIGO Scientific Collaboration & VIRGO Collaboration 2019a). On May 10, 20:43:51 UTC the classification of the nature of the event was updated to 85% BNS and 15% nonastrophysical. Finally at 20:18:44 UTC on May 11, the LVC updated this probability to being of a nonastrophysical origin at 58% and of a BNS to 42% as well as updating the false alarm rate to 1 in 3.6 yr.

### 2.2. DECam Observations

DECam was used for two nights to conduct target-of-opportunity imaging of the LIGO/Virgo GW compact binary merger candidate S190510g (LIGO Scientific Collaboration & VIRGO Collaboration 2019b). Since the initial classification of S190510g was a BNS merger with high probability, the GROWTH collaboration chose to trigger DECam (NOAO proposal 2019A-0205). All exposures from this proposal were immediately made public (Andreoni et al. 2019b). GROWTH initiated EM follow-up on 2019 May 10 at 06:00:25.488 UTC. The observing plan on this evening was based on the original LVC bayestar probability map. The updated LVC LALInference map disfavored most of the region observed on the first night. As a result GROWTH prepared a new observing plan for the second night (Andreoni et al. 2019b). This plan consisted of observing for ∼1.5 hr beginning at 22:51:57 UTC on 2019 May 10. Eighty exposures total were taken in the $g$, $r$, and $z$ bands for 40 s each. Each filter visited roughly the same area of the sky, approximately 30 minutes apart, in order to eliminate moving objects. The $10\sigma$ depths for each band are $m_z = 20.58$ mag, $m_r = 21.72$ mag, and $m_g = 21.67$ mag, where the average seeing was $1\farcs33$, the average airmass was 1.71, and the average attenuation due to cloud was 4%. These observations covered ∼65% of the probability region, as shown in Figure 1. Plans to follow-up this event for a third night were retracted due to the updated classification probability of this event. Our analysis uses only the exposures from the second night of observations as to include only the high probability region from the LALInference LVC map.

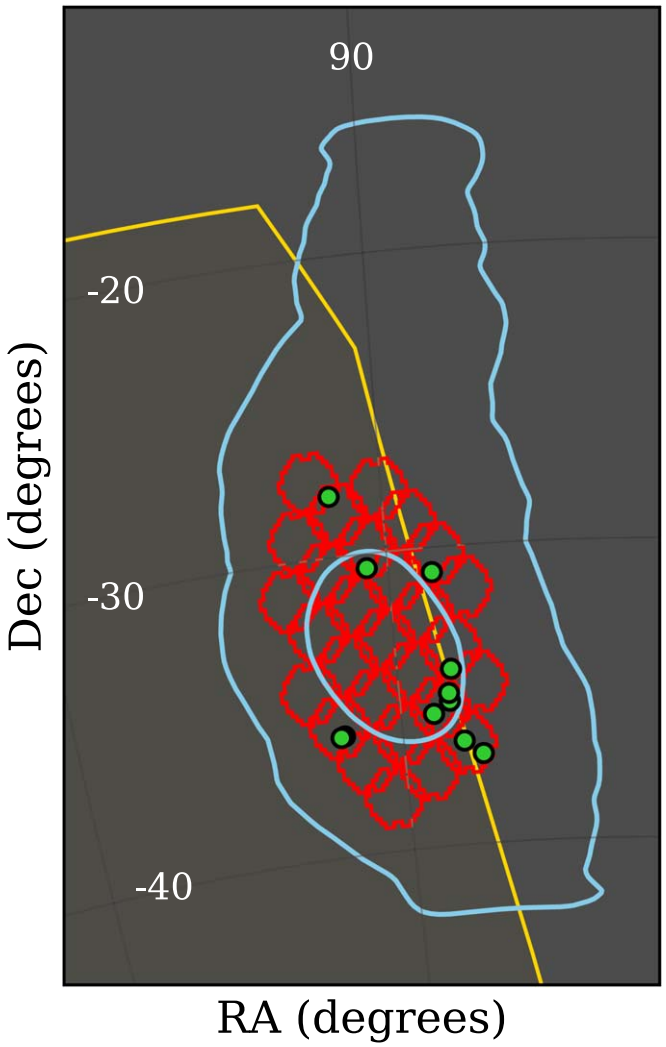


**Figure 1.** Summary of candidates identified by the DESGW short latency pipeline and exposures used for analysis. Here we show one of the three distinct localization regions from the LALInference map. The blue contours show a single region of the LVC 90% and 50% localization contours, the yellow line and shaded area is the DES footprint, and green dots indicate our candidates. A single pointing of DECam exposures are shown as red hexes, which cover ∼84 $\mathrm{deg}^2$ total and contain ∼65% of the total probability.

## 3. Methods

### 3.1. Search and Discovery Pipeline

Images from DECam were downloaded directly to Fermi National Accelerator Laboratory from Cerro Tololo Inter-American Observatory (CTIO) via the National Center for Supercomputing Applications (NCSA). Once the search exposures became available, we immediately started initial image processing, parallelized to run on a CCD by CCD basis,

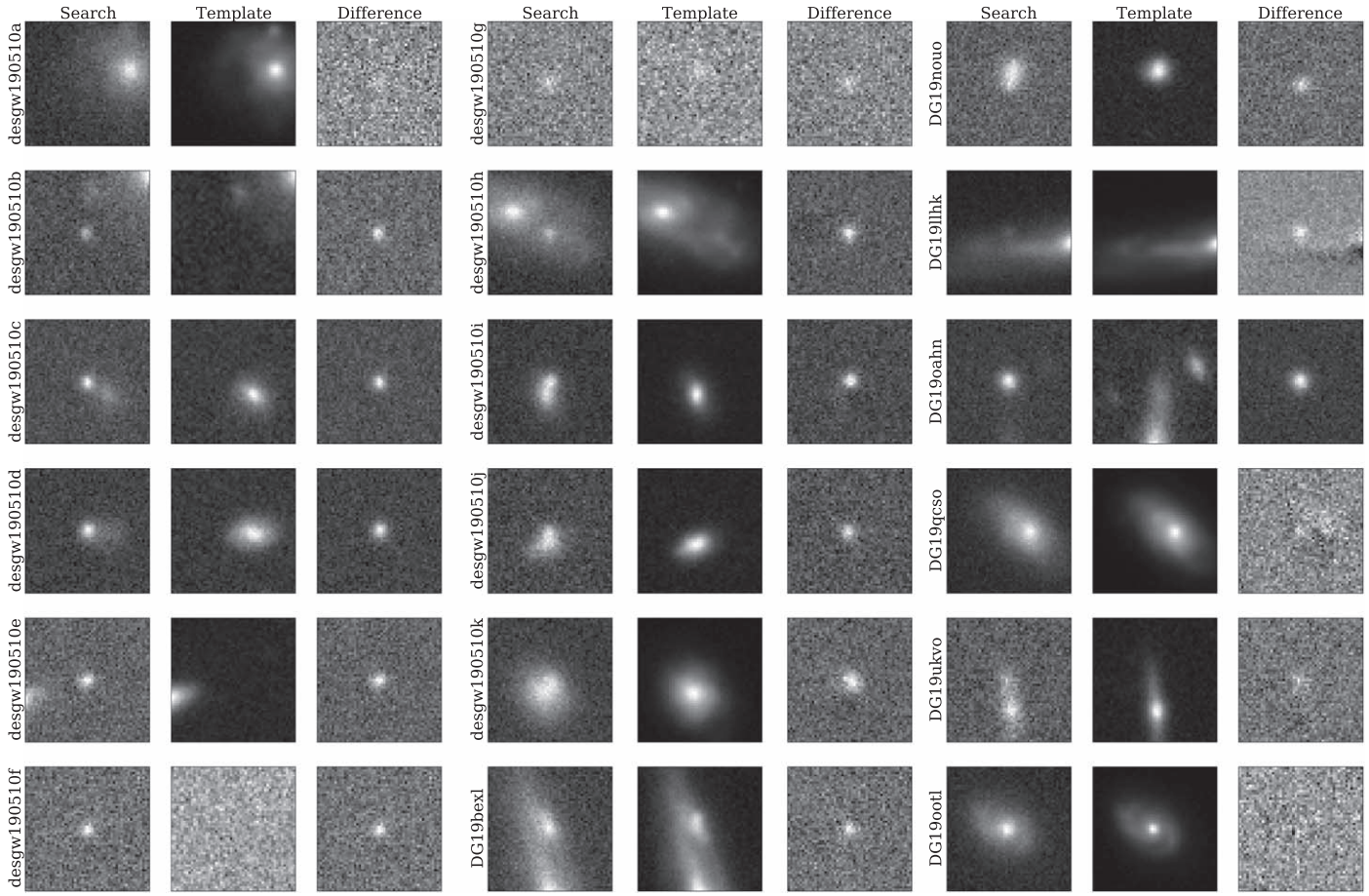


**Figure 2.** Stamps (search, template, and difference images) for all S190510g candidates found by DESGW, including 11 candidates detected in our short latency search (as reported in GCN 24480) and 7 candidates that were first reported by the GROWTH collaboration. Six of the GROWTH candidates were later found by our pipeline, while DG19ootl was not.

via the DESGW Search and Discovery Pipeline (Herner et al. 2020). The pipeline consists of three major stages: Single-Epoch (SE) processing, difference imaging, and post-processing.

SE processing (Morganson et al. 2018) consists of image correction and astrometric calibration. This stage uses `SExtractor` (Bertin & Arnouts 1996) to create a list of bright objects in each image, which is fed into `scamp` for astrometric calibration (Bertin 2006). We use the GAIA-DR2 catalog (Gaia Collaboration, et al. 2016, 2018) in this stage, which allows reductions of DES astrometric uncertainties to below $0.03''$. The outputs of SE processing are the inputs to the difference imaging (`diffimg`) stage, designed for the DES supernova `diffimg` pipeline (Kessler et al. 2015), but modified to work with wide-survey images. `Diffimg` subtracts one or more template images from the search image. Template images are taken in the same area of sky before the event, or after the event is expected to have faded if preexisting templates are unavailable. Our group is able to use all DES images as templates, including those not yet publicly released, as well as all public non-DES DECam images. Combining public DECam data and not-yet-released DES data, we are able to improve on the depth of template images by roughly $\sim\sqrt{2}$ within the DES footprint. After the `diffimg` subtraction is complete, post-processing takes candidate objects identified and applies a cut based on the machine-learning algorithm (`autoscan`) score (Goldstein et al. 2015a, 2015b). Furthermore, forced photometry (described in Kessler et al. (2015)) is applied in this step, as well as host galaxy matching and additional requirements such as detections in multiple bands and/or on multiple nights. For S190510g, these requirements were only a detection in two or more exposures and a machine-learning score adequate to reject nonastrophysical sources. We eliminated known asteroids using the minor planet center, but since a second night of exposures were not taken in the region of interest, we did not eliminate other asteroids from our candidate list. Finally, the resulting candidate list was vetted via human inspection, as described in Section 3.2. The stamps for each of the DESGW candidates are shown in Figure 2.

#### *3.1.1. Pipeline Performance*

Roughly 26% of the image processing jobs took between $0–30^{\rm min}$ to complete, 23% took $0.5–1^{\rm hr}$, 22% took $1–1.5^{\rm hr}$, and 14% took $1.5–2^{\rm hr}$, while the rest took $>2^{\rm hr}$ to complete. The image processing section of our pipeline runs on a parallelized CCD per CCD basis. This means that for the 80 exposures used for this analysis, there were ∼5000 jobs total. Post-processing also runs on a CCD per CCD basis after image processing has finished. This step takes ∼20 minutes to finish when running with all exposures. We note that this turnaround time is significantly longer than the GROWTH team reported in

**Table 1**
Candidates That Pass the DESGW Pipeline Cuts as Well as Visual Inspection from the First Stage of Analysis

| DES (GROWTH) Name | mag $g$ | mag $r$ | mag $z$ | R.A. (deg) | Decl. (deg) | autoscan Score | Classification |
|---|---|---|---|---|---|---|---|
| desgw-190510a | 22.53 ± 0.19 | 20.93 ± 0.04 | 20.77 ± 0.10 | 91.526744 | −35.541616 | 0.950 | SN |
| desgw-190510b | 21.19 ± 0.05 | 21.13 ± 0.05 | | 93.704382 | −36.980727 | 0.950 | |
| desgw-190510c (DG19fqqk) | 21.72 ± 0.1 | 20.37 ± 0.02 | 20.35 ± 0.06 | 92.851468 | −36.517324 | 0.970 | SN II |
| desgw-190510d (DG19nanl) | 20.36 ± 0.03 | 19.92 ± 0.2 | 20.77 ± 0.11 | 87.311398 | −35.955853 | 0.970 | |
| desgw-190510e (DG19etsk) | 20.56 ± 0.03 | 20.66 ± 0.03 | 20.82 ± 0.09 | 89.100926 | −30.473987 | 0.970 | |
| desgw-190510f | 22.16 ± 0.13 | 21.30 ± 0.05 | | 92.294458 | −34.884684 | 0.970 | |
| desgw-190510g | 22.48 ± 0.17 | 21.92 ± 0.09 | | 92.468923 | −34.08657 | 0.963 | |
| desgw-190510h | 21.23 ± 0.08 | 20.29 ± 0.03 | 20.56 ± 0.07 | 87.762354 | −27.956502 | 0.960 | SN |
| desgw-190510i (DG19yhhm) | | 20.15 ± 0.02 | 20.47 ± 0.08 | 91.936973 | −30.824747 | 0.915 | SN |
| desgw-190510j (DG19zaxn) | 20.65 ± 0.04 | 20.83 ± 0.04 | | 92.307977 | −35.149829 | 0.900 | SN |
| desgw-190510k (DG19lcnl) | 20.15 ± 0.03 | | 19.53 ± 0.03 | 87.146843 | −35.994357 | 0.920 | SN |

**Note.** If the candidate matches a candidate from the GROWTH team's candidate list, the GROWTH name is stated. If additional follow-up conducted by other telescopes verified the candidate as SN the classification is listed. Those labeled only "SN" did not have sufficient information for specific classification.

Andreoni et al. (2019b). This is likely due to a combination of having, on average, more template images and applying a more complete correction set in the SE stage, such as correcting for the brighter-fatter effect (Bernstein et al. 2017).

### 3.2. Candidate Identification

In total, there were 1165 candidates identified after post-processing. The final candidate list was published in GCN 24480 at 12:24 pm 2019 May 11 UTC (Soares-Santos 2019). The primary cuts for our candidates require no SExtractor errors in image processing, such as masking of objects overlapping the transient or inability to measure the flux, and an autoscan score of at least 0.9 out of 1.0. This cut found 96 candidates (20 with autoscan score >0.95), while the final 11 were selected via visual inspection. The key properties we looked for when performing visual inspection is a host galaxy in the template image, a non-noisy template image, and no regions of over- or under-subtraction. We also took into consideration the possibility that the candidate could be an AGN since we are unable to resolve objects that are close to the center of the host galaxy and therefore disfavored stamps where the candidate is not distinguishable from the host galaxy. Further, we note that no candidate from our pipeline is fully dismissed until there is secondary follow-up or enough evidence to definitively categorize the object. For a single night of observations, our goal is to rapidly identify objects that are the most obvious candidates, then refine our search criteria as we observe more epochs.

Additionally, we matched candidates to hosts and used DES data to measure properties of the host, such as photometric redshift, absolute magnitude, stellar mass, and star formation rate, as well as the separation of the candidate and the host at the redshift of the nearest potential host galaxy. Photometric redshifts have been computed using Directional Neighborhood Fitting (DNF; De Vicente et al. 2016), while the galaxy properties have been computed using the Bayesian Model Averaging method as described in Palmese et al. (2020b). The coordinates and other information about each of our candidates can be found in Table 1, and information about their host galaxies is listed in Table 2.

## 4. Results

### 4.1. Candidate Classification

The first stage of analysis, performed as exposures became available, presented 11 candidates (of which six were also detected by GROWTH) that were produced via the DESGW Search and Discovery Pipeline discussed in Section 3. Follow-up from other observatories is crucial for determining if a candidate is the GW counterpart through rejection of false positives. The Korea Microlensing Telescope Network (KMTNet) followed-up five of our candidates, desgw-190510a, desgw-190510c, desgw-190510i, desgw-190510j, and desgw-190510k (GCN 24493 and 24529; Im et al. 2019a, 2019b), at the KMTNet South Africa (SAAO), Chile (CTIO), and Australia (SSO) stations showing that each of these candidates did not have significant fading over ∼1 day, but did show very slow or no fading, therefore deeming these candidates likely supernovae. Additionally desgw-190510c was observed by Swift-XRT (GCN 24541; Evans et al. 2019), showing no XRT source found, as well as with Magellan (GCN 24511; Gomez et al. 2019), which found a broad feature consistent with H-$\alpha$ at a redshift of 0.06 and suggests a good match to a Type II SN approximately one week after peak brightness. Finally, desgw-190510h was initially detected by ATLAS on 2019 March 13 and later classified as a Type Ia SN at redshift 0.07 roughly a few days after maximum light by the Spectral Classification of Astronomical Transients (SCAT) survey and desgw190510-b was recorded by Gaia on 2019 January 30 and reported as a "blue hostless transient." This transient can also be seen in previous DES images dating about 2.5 yr ago, though with not enough information to classify it with certainty, thus we provide no host information in Table 2. This leaves only four candidates, desgw-190510d, e, f, and g, that were not classified by secondary follow-up, and thus still potential counterpart candidates.

The remaining information about each candidate that can be used to determine if a candidate is viable can be found in Table 2. The table reports photometric redshift, star formation rate, stellar mass, and absolute magnitude of the hosts, computed using DES Year 3 data (Abbott et al. 2018b). Furthermore, galaxies are ranked based on their probability of association, which can be computed using the skymap

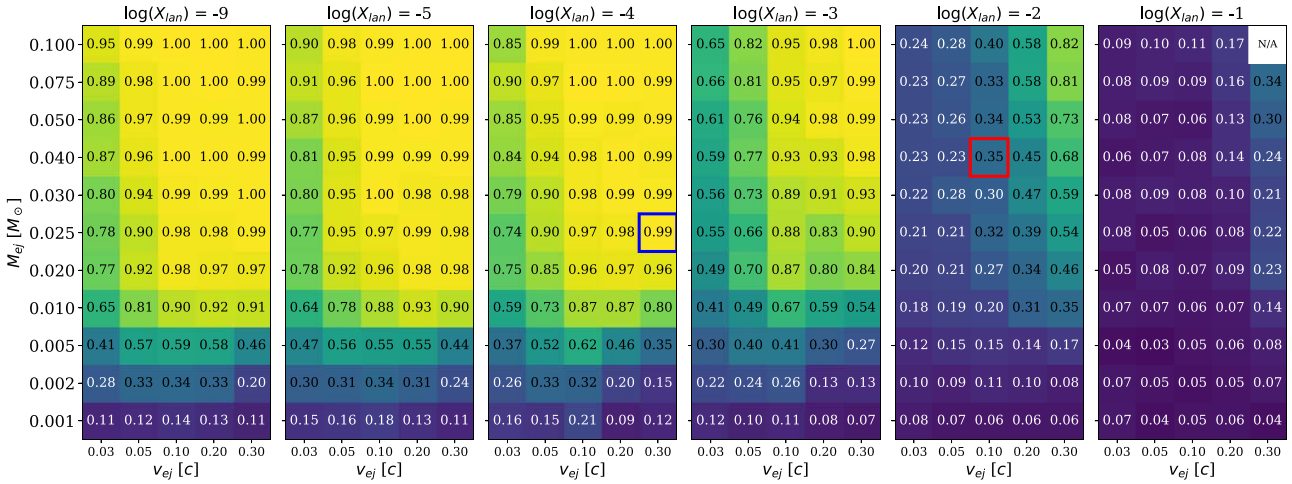


**Figure 3.** Summary of detectable kilonovae given the observing conditions of 2019 May 11. Simulations are set within the LVC distance range of S190510g. Parameters determining the components of the KN, ejecta mass ($M_{\rm ej}$), ejecta velocity ($v_{\rm ej}$), and the log of lanthanide ($\log X_{\rm lan}$) fraction, are taken from Kasen et al. (2017). The coloring and labeling in each box denotes how likely we would be able to detect a KN with the given parameters assuming the event is within our observations. The box labeled "N/A" is a combination of parameters not available in the Kasen et al. (2017) parameters. Additionally, we highlight the set of parameters that were identified as the likely red and blue component of GW170817 as red and blue boxes.

**Table 2**
Candidate Host Galaxies' Information

| Name | Host Gal. Name | Sep (kpc) | $z$ | Log($M_\star$) Log(($M_\odot$)) | Log(SFR) Log(($M_\odot$yr$^{-1}$)) | $M_i$ | Rank |
|---|---|---|---|---|---|---|---|
| desgw-190510a | 2MASS J06060625-3532351 | 32.1 | 0.106 ± 0.004 | $11.069^{+0.19}_{-0.05}$ | −0.190 | −23.043 | 3 |
| desgw-190510b | | | | | | | |
| desgw-190510c | DES J061124.4562-363104.494 | 97.7 | 0.202 ± 0.098 | $9.028^{+0.055}_{-0.060}$ | −0.462 | −20.071 | 9 |
| desgw-190510d | WISEA J054914.81-355724.3 | 5.0 | 0.130 ± 0.021 | $9.388^{+0.14}_{-0.09}$ | −0.502 | −19.33 | 4 |
| desgw-190510e | WISEA J055624.41-302817.8 | 24.6 | 0.163 ± 0.005 | $10.829^{+0.05}_{-0.12}$ | −0.390 | −21.796 | 8 |
| desgw-190510f | 2MASS J06091226-3452506 | 68.9 | 0.168 ± 0.003 | $11.200^{+0.034}_{-0.034}$ | −0.156 | −22.685 | 7 |
| desgw-190510g | DES J060952.4784-340540.704 | 218.3 | 0.575 ± 0.174 | $9.517^{+0.17}_{-0.14}$ | 0.259 | −20.557 | 10 |
| desgw-190510h | 2MASS J05510277-2757201 | 4.3 | 0.049 ± 0.002 | $10.004^{+0.034}_{-0.052}$ | −1.388 | −20.917 | 1 |
| desgw-190510i | WISEA J060745.00-304928.7 | 55.7 | 0.193 ± 0.019 | $10.341^{+0.052}_{-0.041}$ | 0.387 | −21.539 | 6 |
| desgw-190510j | WISEA J060914.02-350858.5 | 3.1 | 0.134 ± 0.014 | $9.69^{+0.14}_{-0.13}$ | −0.461 | −19.927 | 5 |
| desgw-190510k | 2MASS J05483537-3559390 | 1.9 | 0.067 ± 0.002 | $9.829^{+0.09}_{-0.20}$ | −0.272 | −20.627 | 2 |

**Note.** Redshifts listed are mean photometric redshifts with 1σ errors. All photometric data, star formation rates (SFR), stellar mass ($M_\star$), and magnitudes are computed using DES Year 3 data. Additionally, the separation ("Sep") between candidate and host galaxy is calculated using the redshift of the galaxy. Galaxies are ranked based on their position in the sky and redshift, using the information provided in the skymap. Log indicates a logarithm in base 10.

information, the galaxies' position, and redshift (Singer et al. 2016), assuming a flat ΛCDM cosmology with $H_0 = 70$ km s$^{-1}$ Mpc$^{-1}$ and $\Omega_m = 0.3$.

### 4.2. Recovered Candidates

Using the same exposures, the GROWTH collaboration reported a list of 13 candidates (GCN 24467; Andreoni et al. 2019a). Seven of the GROWTH candidates were not listed in the initial DESGW candidate list reported in GCN 24480. Candidates DG19bexl and DG19nouo were found in the final stages by our automated pipeline; DG19bexl did not pass the `autoScan` score cut (⩾0.9) and DG19nouo was rejected due to visual inspection. Candidates DS19qcso and DG19llhk both had a detection in a single exposure, where two were required to be picked up as a candidate. The overlapping search exposures for these candidates failed in the `HOTPANTS` step of our pipeline. Reprocessing of these exposures with an updated (current) version of the DESGW pipeline did identify these candidates. Similarly, candidates DG19ukvo and DG19oahn were not found in our initial processing of the event due to `HOTPANTS` errors in all exposures. DG19oahn was later found in reprocessing, while DG19ukvo continued to have processing failures in two out of the three exposures. The fraction of missing candidates is consistent with the overall failure rate of 28% for all jobs that were submitted on that night, where ∼15% of total jobs failed due to issues in `HOTPANTS`. These failures are largely due to the observing conditions described in Section 2.2. Finally, candidate DG19ootl was never found in our pipeline. The templates used for this exposure were taken from not yet publicly available DES images and thus did not show any source in the difference image. Candidates, including those initially detected only by GROWTH, are shown in Figure 2.

## 5. Discussion

### 5.1. Understanding Search Efficiency

To better understand our search efficiency, we performed an offline analysis using SuperNova ANAlysis software suite (SNANA) (Kessler et al. 2009). These simulations produce SN

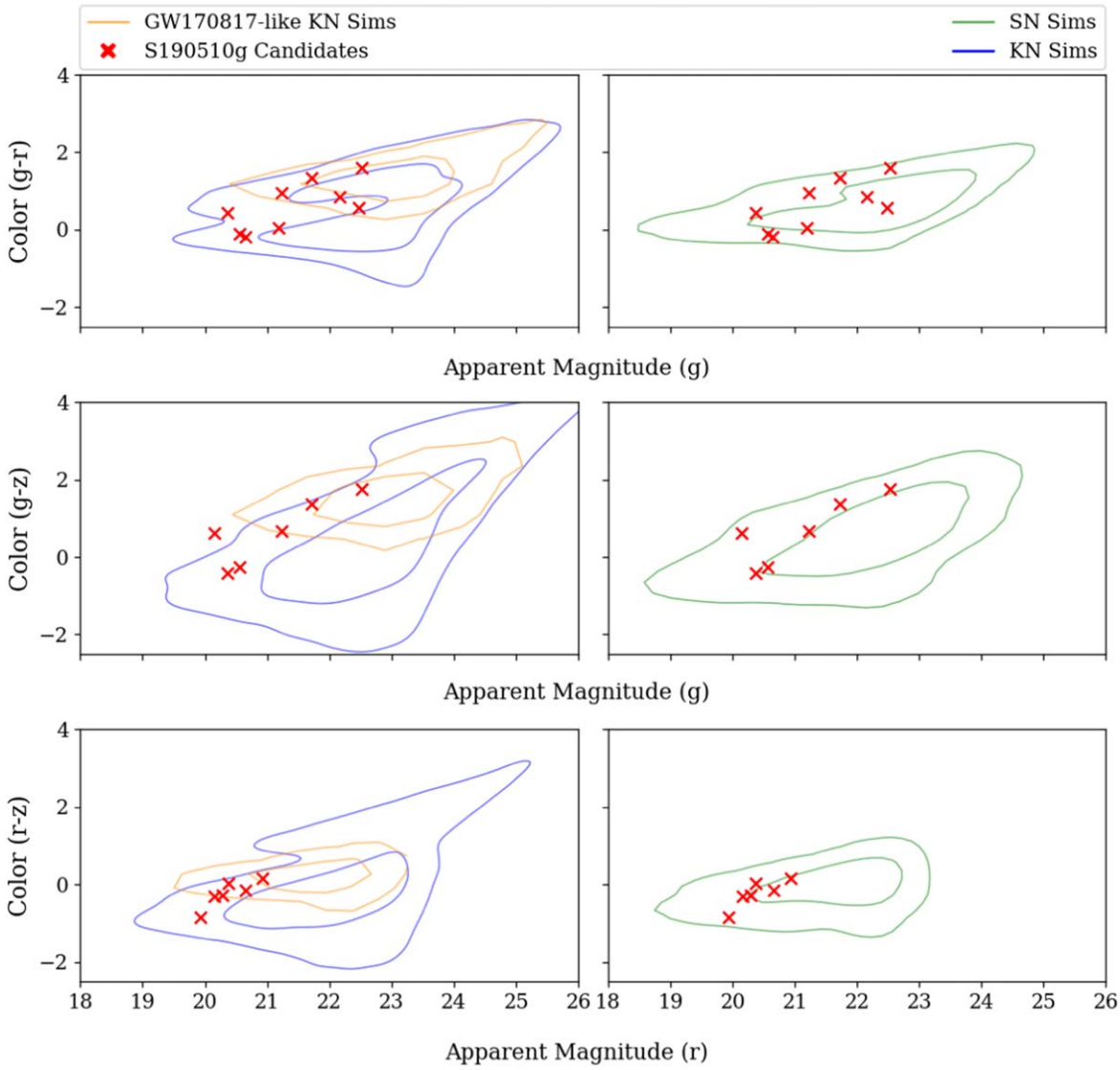


**Figure 4.** DESGW candidates (red) as compared to where kilonovae and supernovae would be expected to live in color–magnitude space given the observing conditions of our observations (i.e., 36 hours after merger, sky brightness, etc.). All simulations run using SNANA (Kessler et al. 2009). Kilonovae simulations were generated with a burst date consistent with that reported by LVC, and at a distance consistent with the LVC distance distribution (blue contours). The KN parameters, ejecta velocity, mass, and lanthanide fraction are randomly selected from the parameters described by Kasen et al. (2017). Simulations with the same Kasen parameters as the blue component of GW170817 (ejecta velocity = 0.3c, lanthanide fraction = $10^{-4}$ and ejecta mass = $0.025M\odot$) are shown as orange contours. Supernovae simulations consist of Type Ia and CC SN, and are generated using a peak date ranging 4 months centered around May 10, with redshift also consistent with S190510g's distance distribution. The contours show 50% and 90% density of simulations.

and KN light curves as they would be observed during our observations. Each KN simulation randomly assigns an ejecta mass, ejecta velocity, and lanthanide fraction based on the Kasen KN model (Kasen et al. 2017), as well as host galaxy extinction between 0 and 3 mag (Cardelli et al. 1989). The SN simulations use the SALT2 model for SN Ia (Guy et al. 2010) and templates for the core collapse SN (SN CC) are taken from Kessler et al. (2010) and Jones et al. (2018). Additionally we note that these light curves are modeled assuming face-on emission of the observed component or spherically symmetric emission. While studies have shown the importance of viewing angle dependence on KN brightness (Dhawan et al. 2020; Kawaguchi et al. 2020; Korobkin et al. 2020), this approach was selected for simplicity.

Using these simulations, we computed the detection efficiency for each KN model given our observing conditions, the results of which are shown in Figure 3. The KN simulations used for this analysis produce events that use a distance distribution consistent with that reported by the LVC as well as being located within the 65% probability area that was surveyed. The efficiency of each model, represents the fraction of light curves that are detected to be brighter than our $5\sigma$ limiting magnitude at the time of DECam observations.

Next, we used these simulations to examine the color–magnitude space for both KN and SN (Figure 4). For this analysis, we use both KN and SN simulations. Here we require the detected object to be brighter than our $5\sigma$ limiting magnitude. Additionally, we require the object's host-galaxy photometric redshift to be consistent with the LVC luminosity distance posterior at the $3\sigma$ confidence level. Additionally, the simulated SNe were distributed in redshift according to the measured volumetric rates of SNe-Ia and SNe-CC.

### 5.2. Implications for Search Efficiency

Figure 3 shows the likelihood that we would have been able to detect a KN produced by this event given the observing conditions and depth of observations. Here we show all possible sets of KN parameters and note that a GW170817-like KN follows a two component model, red and blue, where the blue component is dominant at early times (i.e., up to ∼2.5 days after merger; Kasen et al. 2017) in the light-curve evolution. Assuming S190510g is a GW170817-like KN viewed from the same orientation located within our exposures, our simulations show that we would have a 99% chance of detecting the counterpart KN. However, a wide range of KN models would have been outside of our sensitivity range and thus unobservable.

While we have the ability to detect such a source, it is challenging to determine a candidate to be KN or SN with a single night of observations in the absence of spectroscopic information. To demonstrate the difficulty of this task we examined the color–magnitude space of the simulated KN and SN events. All KN simulations are shown as the blue contours (indicating 50% and 90% density of simulations) in the left panel of Figure 4, with the parameters for the blue component of GW170817 (ejecta velocity = 0.3c, lanthanide fraction = $10^{-4}$, ejecta mass = $0.025M\odot$, and assuming spherically symmetric emission) highlighted as orange contours. Meanwhile the color–magnitude distribution of SN simulations is shown by the green contour on the right panel of Figure 4. All DESGW S190510g candidates from this event (depicted as red crosses in Figure 4) fall within the possible 90% color–magnitude regions of SN events. For a KN roughly one day after burst, and given only this color–magnitude information, each of these candidates could be either an SN or a KN.

### 5.3. Implications for Follow-up Strategy

In the first half of the O3 observing run, most of the events that included a neutron star did not have a good localization (i.e., hundreds of deg$^2$) as well as being far away (>200 Mpc) when compared to GW170817. While it would be ideal to cover 100% of the localization area with multiple filters, limited telescope time and poor localization maps make this very challenging. In the following, we show that prioritizing sufficiently deep images as opposed to covering large areas and/or using multiple filters, will result in a higher chance of detecting counterparts.

To show how many events it would take to have a 50% (99%) chance of detecting one counterpart, we have to consider the cumulative probability inside the LVC localization map that was observed ($\Sigma_{\rm spatial}$), the fraction of DECam that was live during observations ($\epsilon_{\rm camera}$), the probability that the event is astrophysical in nature ($\epsilon_{\rm real}$), and our likelihood of being able to detect a KN at that distance given the observing conditions (i.e., the fraction of simulated light curves that are brighter than our $5\sigma$ depth) ($\epsilon_{\rm efficiency}$)

$$P_i = \Sigma_{\rm spatial} \times \epsilon_{\rm camera} \times \epsilon_{\rm efficiency} \times \epsilon_{\rm real} \quad (1)$$

$$P_{\rm one} = 1 - \prod_i^N (1 - P_i) \quad (2)$$

Here, $_{Pi}$ is the probability of being able to detect a KN from a single GW event. $P_{\rm one}$ is the cumulative probability of being able to detect a single counterpart given $N$ GW events (Annis & Soares-Santos 2016). For this calculation, we find that if we assume there is a kilonova associated with S190510g that is GW170817-like, i.e., $\epsilon_{\rm efficiency} = 0.993$, we would need to observe 3 (19) identical events with $\Sigma_{\rm spatial} = 0.65$, $\epsilon_{\rm camera} = 0.8$, $\epsilon_{\rm real} = 0.42$, and $\epsilon_{\rm efficiency} = 0.993$ in order to have 50% (99%) probability of identifying the event using the current strategy. Since there is no way of knowing that the event will have a light curve similar to GW170817, we also calculate this using the average efficiency value of all KN parameters, $\epsilon_{\rm efficiency} = 0.553$, with all other parameters the same. Here we find that we would need 6 (36) events to reach 50% (99%) likelihood of detecting the counterpart.

We then repeat this calculation assuming the observing strategy uses one filter instead of three. If we conserve the telescope time used and area surveyed per event, we can then increase the exposure time from 40 to 170 s. In this scenario, the efficiency for a GW170817-like KN is 0.995, meaning we would again need 3 (19) events to have 50% (99%) likelihood of detection. Using the average efficiency in this scenario though, 0.742, we would only need 4 (27) events to have 50% (99%) likelihood of detecting a counterpart. By increasing the depth of our observations, we become sensitive to more KN models and will thus need to observe fewer total GW events to have a high probability of making a detection.

## 6. Conclusion

We performed a follow-up analysis of the GW trigger S190510g, using DECam target of opportunity time data from 2019 May 11. We demonstrated the DESGW team's ability to quickly process new images in real time, averaging ∼1 hr for image processing to complete. The final DESGW candidate list is summarized in Table 1, with five candidates, desgw-190510a, c, i, j, and k being ruled out due to secondary follow-up efforts by KMTNet, Swift-XRT, and Magellan. Similarly, candidates desgw-190510b and h have been identified based on previous observation as recorded in the Transient Name Server. This leaves four candidates from the DESGW candidate list that were not classified by secondary follow-up. Each of these candidates have color information that is consistent with SN.

Additionally, we used simulated KN to show the efficiency of detecting a KN counterpart given the observing conditions of the observations to find that we have a 99% chance of being able to detect a KN counterpart assuming the light curve has the same physical parameters as GW170817 using the Kasen et al. (2017) model (Figure 3) within our observations. However, this efficiency is not uniform across all KN models. We also used KN and SN simulations to study where in color–magnitude space they land. We find that all of our candidates are consistent with both KN and SN using this metric.

To make ourselves more sensitive to all KN models, we suggest prioritizing longer exposure times over multiple filters and covering large portions of the localization area for future observations. Using exposures that are 4 times longer than those used for this follow-up, we would only need to observe four events (identical to S190510g) to have a 50% chance of detecting a KN counterpart within the 65% probability region observed and with these observing conditions, compared to the six events needed using the current strategy.

Funding for the DES Projects has been provided by the U.S. Department of Energy, the U.S. National Science Foundation, the Ministry of Science and Education of Spain, the Science and Technology Facilities Council of the United Kingdom, the

Higher Education Funding Council for England, the National Center for Supercomputing Applications at the University of Illinois at Urbana-Champaign, the Kavli Institute of Cosmological Physics at the University of Chicago, the Center for Cosmology and Astro-Particle Physics at the Ohio State University, the Mitchell Institute for Fundamental Physics and Astronomy at Texas A&M University, Financiadora de Estudos e Projetos, Fundação Carlos Chagas Filho de Amparo à Pesquisa do Estado do Rio de Janeiro, Conselho Nacional de Desenvolvimento Científico e Tecnológico and the Ministério da Ciência, Tecnologia e Inovação, the Deutsche Forschungsgemeinschaft and the Collaborating Institutions in the Dark Energy Survey.

The Collaborating Institutions are Argonne National Laboratory, the University of California at Santa Cruz, the University of Cambridge, Centro de Investigaciones Energéticas, Medioambientales y Tecnológicas-Madrid, the University of Chicago, University College London, the DES-Brazil Consortium, the University of Edinburgh, the Eidgenössische Technische Hochschule (ETH) Zürich, Fermi National Accelerator Laboratory, the University of Illinois at Urbana-Champaign, the Institut de Ciències de l'Espai (IEEC/CSIC), the Institut de Física d'Altes Energies, Lawrence Berkeley National Laboratory, the Ludwig-Maximilians Universität München and the associated Excellence Cluster Universe, the University of Michigan, NFS's NOIRLab, the University of Nottingham, The Ohio State University, the University of Pennsylvania, the University of Portsmouth, SLAC National Accelerator Laboratory, Stanford University, the University of Sussex, Texas A&M University, and the OzDES Membership Consortium.

Based in part on observations at Cerro Tololo Inter-American Observatory at NSFs NOIRLab (NOIRLab Prop. ID 2012B-0001; PI: J. Frieman), which is managed by the Association of Universities for Research in Astronomy (AURA) under a cooperative agreement with the National Science Foundation.

The DES data management system is supported by the National Science Foundation under grant Nos. AST-1138766 and AST-1536171. The DES participants from Spanish institutions are partially supported by MICINN under grants ESP2017-89838, PGC2018-094773, PGC2018-102021, SEV-2016-0588, SEV-2016-0597, and MDM-2015-0509, some of which include ERDF funds from the European Union. IFAE is partially funded by the CERCA program of the Generalitat de Catalunya. Research leading to these results has received funding from the European Research Council under the European Union's Seventh Framework Program (FP7/2007–2013) including ERC grant agreements 240672, 291329, and 306478. We acknowledge support from the Brazilian Instituto Nacional de Ciência e Tecnologia (INCT) e-Universe (CNPq grant 465376/2014-2).

This manuscript has been authored by Fermi Research Alliance, LLC under Contract No. DE-AC02-07CH11359 with the U.S. Department of Energy, Office of Science, Office of High Energy Physics.

This material is based upon work supported by the National Science Foundation Graduate Research Fellowship Program under grant No. 1744555. Any opinions, findings, and conclusions or recommendations expressed in this material are those of the author(s) and do not necessarily reflect the views of the National Science Foundation.

R.M. thanks the LSSTC Data Science Fellowship Program, which is funded by LSSTC, NSF Cybertraining grant #1829740, the Brinson Foundation, and the Moore Foundation; his participation in the program has benefited this work.

F.O.E. acknowledges support from the FONDECYT grant No. 1201223.

## ORCID iDs

A. Garcia https://orcid.org/0000-0001-9578-6322
R. Morgan https://orcid.org/0000-0002-7016-5471
K. Herner https://orcid.org/0000-0001-6718-2978
A. Palmese https://orcid.org/0000-0002-6011-0530
M. Soares-Santos https://orcid.org/0000-0001-6082-8529
J. Annis https://orcid.org/0000-0002-0609-3987
D. Brout https://orcid.org/0000-0001-5201-8374
A. K. Vivas https://orcid.org/0000-0003-4341-6172
A. Drlica-Wagner https://orcid.org/0000-0001-8251-933X
L. Santana-Silva https://orcid.org/0000-0003-3402-6164
D. L. Tucker https://orcid.org/0000-0001-7211-5729
S. Allam https://orcid.org/0000-0002-7069-7857
M. Wiesner https://orcid.org/0000-0001-8653-7738
J. García-Bellido https://orcid.org/0000-0002-9370-8360
M. S. S. Gill https://orcid.org/0000-0003-2524-5154
R. Kessler https://orcid.org/0000-0003-3221-0419
T. M. Davis https://orcid.org/0000-0002-4213-8783
J. Casares https://orcid.org/0000-0001-5031-0128
C. Conselice https://orcid.org/0000-0003-1949-7638
J. Cooke https://orcid.org/0000-0001-5703-2108
Z. Doctor https://orcid.org/0000-0002-2077-4914
D. A. Howell https://orcid.org/0000-0003-4253-656X
C. Lidman https://orcid.org/0000-0003-1731-0497
F. Olivares E. https://orcid.org/0000-0002-5115-6377
A. Rest https://orcid.org/0000-0002-4410-5387
N. Sherman https://orcid.org/0000-0001-5399-0114
D. Brooks https://orcid.org/0000-0002-8458-5047
A. Carnero Rosell https://orcid.org/0000-0003-3044-5150
M. Carrasco Kind https://orcid.org/0000-0002-4802-3194
J. Carretero https://orcid.org/0000-0002-3130-0204
S. Desai https://orcid.org/0000-0002-0466-3288
H. T. Diehl https://orcid.org/0000-0002-8357-7467
J. P. Dietrich https://orcid.org/0000-0002-8134-9591
B. Flaugher https://orcid.org/0000-0002-2367-5049
D. Friedel https://orcid.org/0000-0002-3632-7668
J. Frieman https://orcid.org/0000-0003-4079-3263
E. Gaztanaga https://orcid.org/0000-0001-9632-0815
D. W. Gerdes https://orcid.org/0000-0001-6942-2736
D. Gruen https://orcid.org/0000-0003-3270-7644
R. A. Gruendl https://orcid.org/0000-0002-4588-6517
J. Gschwend https://orcid.org/0000-0003-3023-8362
G. Gutierrez https://orcid.org/0000-0003-0825-0517
S. R. Hinton https://orcid.org/0000-0003-2071-9349
D. L. Hollowood https://orcid.org/0000-0002-9369-4157
K. Honscheid https://orcid.org/0000-0002-6550-2023
D. J. James https://orcid.org/0000-0001-5160-4486
K. Kuehn https://orcid.org/0000-0003-0120-0808
N. Kuropatkin https://orcid.org/0000-0003-2511-0946
O. Lahav https://orcid.org/0000-0002-1134-9035
M. A. G. Maia https://orcid.org/0000-0001-9856-9307
J. L. Marshall https://orcid.org/0000-0003-0710-9474
F. Menanteau https://orcid.org/0000-0002-1372-2534
R. Miquel https://orcid.org/0000-0002-6610-4836
R. L. C. Ogando https://orcid.org/0000-0003-2120-1154

A. A. Plazas https://orcid.org/0000-0002-2598-0514
A. K. Romer https://orcid.org/0000-0002-9328-879X
A. Roodman https://orcid.org/0000-0001-5326-3486
E. Sanchez https://orcid.org/0000-0002-9646-8198
M. Schubnell https://orcid.org/0000-0001-9504-2059
I. Sevilla-Noarbe https://orcid.org/0000-0002-1831-1953
M. Smith https://orcid.org/0000-0002-3321-1432
E. Suchyta https://orcid.org/0000-0002-7047-9358
G. Tarle https://orcid.org/0000-0003-1704-0781
A. R. Walker https://orcid.org/0000-0002-7123-8943
J. Weller https://orcid.org/0000-0002-8282-2010

## References

Aasi, J., Abbott, B. P., Abbott, R., et al. 2015, CQGra, 32, 074001
Abbott, B., Abbott, R., Abbott, T., et al. 2019, PhRvX, 9, 031040
Abbott, B. P., Abbott, R., Abbott, T., et al. 2017a, ApJL, 848, L12
Abbott, B. P., Abbott, R., Abbott, T., et al. 2018a, LRR, 21, 3
Abbott, B. P., Abbott, R., Abbott, T. D., et al. 2017b, Natur, 551, 85
Abbott, B. P., Abbott, R., Abbott, T. D., et al. 2017c, PhRvL, 119, 161101
Abbott, T. M. C., Abdalla, F. B., Allam, S., et al. 2018b, ApJS, 239, 18
Andreoni, I., Ackley, K., Cooke, J., et al. 2017, PASA, 34, e069
Andreoni, I., Goldstein, D. A., Anand, S., et al. 2019a, GCN, 24467, 1
Andreoni, I., Goldstein, D. A., Anand, S., et al. 2019b, ApJL, 881, L16
Andreoni, I., Goldstein, D. A., Kasliwal, M. M., et al. 2020a, ApJ, 890, 131
Andreoni, I., Kool, E. C., Sagues Carracedo, A., et al. 2020b, arXiv:2008.00008
Annis, J., & Soares-Santos, M. 2016, arXiv:1609.09517
Bernstein, G., Abbott, T., Desai, S., et al. 2017, PASP, 129, 114502
Bertin, E. 2006, in ASP Conf. Ser., 351, Automatic Astrometric and Photometric Calibration with SCAMP, ed. C. Gabriel (San Francisco, CA: ASP), 112
Bertin, E., & Arnouts, S. 1996, A&AS, 117, 393
Blanchard, P. K., Berger, E., Fong, W., et al. 2017, ApJL, 848, L22
Cardelli, J. A., Clayton, G. C., & Mathis, J. S. 1989, ApJ, 345, 245
Caron, B., Dominjon, A., Drezen, C., et al. 1999, CQGra, 14, 1461
Carracedo, A. S., Bulla, M., Feindt, U., & Goobar, A. 2020, arXiv:2004.06137
Coulter, D., Foley, R., Kilpatrick, C., et al. 2017, Sci, 358, 1556
Cowperthwaite, P., Berger, E., Villar, V., et al. 2017, ApJL, 848, L17
Dark Energy Survey Collaboration, Abbott, T., Abdalla, F. B., et al. 2016, MNRAS, 460, 1270
De Vicente, J., Sánchez, E., & Sevilla-Noarbe, I. 2016, MNRAS, 459, 3078
Del Pozzo, W. 2012, PhRvD, 86, 043011
Dhawan, S., Bulla, M., Goobar, A., Sagués Carracedo, A., & Setzer, C. N. 2020, ApJ, 888, 67
Evans, P., Cenko, S., Kennea, J. A., et al. 2017, Sci, 358, 1565
Evans, P. A., Kennea, J. A., Tohuvavohu, A., et al. 2019, GCN, 24541, 1
Flaugher, B., Diehl, H., Honscheid, K., et al. 2015, AJ, 150, 150
Gaia Collaboration, Brown, A. G. A., Vallenari, A., et al. 2018, A&A, 616, A1
Gaia Collaboration, Prusti, T., de Bruijne, J. H. J., et al. 2016, A&A, 595, A1
Goldstein, D. A., Andreoni, I., Nugent, P. E., et al. 2019, ApJL, 881, L7
Goldstein, D. A., D'Andrea, C. B., Fischer, J. A., et al. 2015a, AJ, 150, 82
Goldstein, D. A., D'Andrea, C. B., Fischer, J. A., et al. 2015b, AJ, 150, 165
Gomez, S., Cowperthwaite, P. S., Hosseinzadeh, G., et al. 2019, GCN, 24511, 1
Guy, J., Sullivan, M., Conley, A., et al. 2010, A&A, 523, A7
Herner, K., Annis, J., Brout, D., et al. 2020, A&C, 33, 100425
Hu, L., Wu, X., Andreoni, I., et al. 2017, SciBu, 62, 1433
Im, M., Kim, J., Lee, C. U., et al. 2019a, GCN, 24493, 1
Im, M., Kim, J., Lee, C. U., et al. 2019b, GCN, 24529, 1
Jones, D. O., Scolnic, D. M., Riess, A. G., et al. 2018, ApJ, 857, 51
Kasen, D., Metzger, B., Barnes, J., Quataert, E., & Ramirez-Ruiz, E. 2017, Natur, 551, 80
Kasliwal, M., Nakar, E., Singer, L., et al. 2017, Sci, 358, 1559
Kasliwal, M. M., Anand, S., Ahumada, T., et al. 2020, arXiv:2006.11306
Kawaguchi, K., Shibata, M., & Tanaka, M. 2020, ApJ, 889, 171
Kessler, R., Bassett, B., Belov, P., et al. 2010, PASP, 122, 1415
Kessler, R., Bernstein, J. P., Cinabro, D., et al. 2009, PASP, 121, 1028
Kessler, R., Marriner, J., Childress, M., et al. 2015, AJ, 150, 172
Korobkin, O., Wollaeger, R., Fryer, C., et al. 2020, arXiv:2004.00102
LIGO Scientific Collaboration & VIRGO Collaboration 2019a, GCN, 24489, 1
LIGO Scientific Collaboration & VIRGO Collaboration 2019b, GCN, 24442, 1
McCully, C., Hiramatsu, D., Howell, D. A., et al. 2017, ApJL, 848, L32
Morgan, R., Soares-Santos, M., Annis, J., et al. 2020, ApJ, 901, 83
Morganson, E., Gruendl, R. A., Menanteau, F., et al. 2018, PASP, 130, 074501
Palmese, A., Annis, J., Burgad, J., et al. 2020b, MNRAS, 493, 4591
Palmese, A., deVicente, J., Pereira, M. E. S., et al. 2020a, ApJL, 900, L33
Palmese, A., Hartley, W., Tarsitano, F., et al. 2017, ApJL, 849, L34
Palmese, A., & Kim, A. G. 2020, arXiv:2005.04325
Schutz, B. F. 1986, Natur, 323, 310
Shappee, B., Simon, J., Drout, M., et al. 2017, Sci, 358, 1574
Singer, L. P., Chen, H.-Y., Holz, D. E., et al. 2016, ApJS, 226, 10
Soares-Santos, M. 2019, GCN, 24480, 1
Soares-Santos, M., Holz, D., Annis, J., et al. 2017, ApJL, 848, L16
Soares-Santos, M., Kessler, R., Berger, E., et al. 2016, ApJL, 823, L33
Soares-Santos, M., Palmese, A., Hartley, W., et al. 2019, ApJL, 876, L7
Utsumi, Y., Tanaka, M., Tominaga, N., et al. 2017, PASJ, 69, 101
Valenti, S., David, J., Yang, S., et al. 2017, ApJL, 848, L24
Veitch, J., Raymond, V., Farr, B., et al. 2015, PhRvD, 91, 042003